Nonlocal correlations in the orbital selective Mott phase of a one-dimensional multiorbital Hubbard model

S. Li,[1] N. Kaushal,[1,5] Y. Wang,[1] Y. Tang,[2] G. Alvarez,[3,4] A. Nocera,[3,4] T. A. Maier,[3,4] E. Dagotto,[1,5] and S. Johnston[1]

[1]*Department of Physics and Astronomy, The University of Tennessee, Knoxville, Tennessee 37996, USA*

[2]*Department of Physics, Virginia Tech, Blacksburg, Virginia 24061, USA*

[3]*Center for Nanophase Materials Sciences, Oak Ridge National Laboratory, Oak Ridge, Tennessee 37831, USA*

[4]*Computer Science and Mathematics Division, Oak Ridge National Laboratory, Oak Ridge, Tennessee 37831, USA*

[5]*Materials Science and Technology Division, Oak Ridge National Laboratory, Oak Ridge, Tennessee 37831, USA*

(Received 15 August 2016; revised manuscript received 15 November 2016; published 12 December 2016)

We study nonlocal correlations in a three-orbital Hubbard model defined on an extended one-dimensional chain using determinant quantum Monte Carlo and density matrix renormalization group methods. We focus on a parameter regime with robust Hund's coupling, which produces an orbital selective Mott phase (OSMP) at intermediate values of the Hubbard U, as well as an orbitally ordered ferromagnetic insulating state at stronger coupling. An examination of the orbital- and spin-correlation functions indicates that the orbital ordering occurs before the onset of magnetic correlations in this parameter regime as a function of temperature. In the OSMP, we find that the self-energy for the itinerant electrons is momentum dependent, indicating a degree of nonlocal correlations while the localized electrons have largely momentum independent self-energies. These nonlocal correlations also produce relative shifts of the holelike and electronlike bands within our model. The overall momentum dependence of these quantities is strongly suppressed in the orbitally ordered insulating phase.

DOI: 10.1103/PhysRevB.94.235126

I. INTRODUCTION

In recent years the scientific community renewed its interest in understanding the properties of multiorbital Hubbard models, and this has been intensified by the discovery of the iron-based superconductors [1–4]. On a theoretical front, this is a challenging problem due to a lack of nonperturbative methods for treating multiorbital Hubbard models at intermediate or strong couplings and on extended systems. Nevertheless, considerable progress has been made using mean-field-based approaches [4–17], resulting in new concepts such as that of a Hund's metal [7,10,18,19] and the orbital-selective Mott phase (OSMP) [10,20]. These concepts are central to understanding the paradoxical appearance of both localized and itinerant characteristics in many multiorbital systems [21,22] and bad metallic behavior in the presence of sizable electronic correlations [22].

The most widely used numerical approach in this context is single-site multiorbital dynamical mean-field theory (DMFT) [4,23,24]. Generally speaking, DMFT maps the full lattice problem onto an impurity problem embedded in an effective medium, which approximates the electron dynamics on a larger length scale as a local renormalization [24]. While this technique has had considerable success in addressing many aspects of the OSMP and other physics related to the multiorbital problem [8,9,12–14,17,25–28], it is unable to capture spatial fluctuations and nonlocal correlations encoded in the k-dependent self-energy $\Sigma(\mathbf{k},\omega)$. This is a potential shortcoming as nonlocal correlations are known to have an impact in the case of the single-band Hubbard model [29,30]. It is therefore necessary to assess the importance of such nonlocal effects on multiorbital properties such as the OSMP.

To date, most nonperturbative studies of nonlocal effects have used cluster DMFT or the dynamical cluster approximation (DCA) [16,31–35]; however, these techniques are typically limited to a handful of sites when multiple orbitals are included in the basis. This is due to technical issues related to each choice in impurity solver, such as the fermion sign problem in the case of quantum Monte Carlo or the exponential growth of the Hilbert space in the case of exact diagonalization. As a result, these studies have only addressed short-range spatial fluctuations. One study of the OSMP has been carried out on a larger two-dimensional cluster using determinant quantum Monte Carlo (DQMC) [36]. In that case, however, the OSMP was imposed by the model by assuming that electrons in a subset of orbitals were localized as Ising spins. In light of these limitations it is desirable to find situations where multiorbital physics can be modeled on extended clusters that support long-range spatial fluctuations and where the properties under study emerge from the underlying many-body physics of the model.

In this regard, one-dimensional (1D) models are quite promising. For example, two recent density matrix renormalization group (DMRG) studies have been carried out for an effective 1D three-orbital model representative of the iron-based superconductors [37,38]. More recently, it was demonstrated that DQMC simulations for a simplified version of the same model can also be carried out to low temperatures due to a surprisingly mild fermion sign problem [39]. These observations open the doorway to nonperturbative studies of this model on extended clusters, thus granting access to the momentum-resolved self-energies and nonlocal correlations. 1D studies along these lines are also directly relevant for the recently discovered quasi-1D selenide $Ba_{1-x}K_xFe_2Se_3$ [40–45]. In this context, it is important to note that DMFT becomes more accurate in higher dimensions and therefore one expects its ability to describe multiorbital Mott physics in 1D to be diminished.

Motivated by these considerations, we examine the properties of a three-orbital Hubbard Hamiltonian on an extended 1D cluster using DQMC and DMRG, with a particular focus

on its k-resolved self-energies and spectral properties. We thus gain explicit access to nonlocal correlations occurring on longer length scales than those addressed in previous nonperturbative studies. In general, we find that the OSMP leads to a mixture of localized and itinerant bands, where the former are characterized by a localized (momentum-independent) self-energy while the latter exhibits significant nonlocal (momentum-dependent) correlations. This leads to a band-dependent relative shift of the underlying electron- and holelike bands. We also identify an insulating state driven by orbital ordering in a region of parameter space previously associated with an OSMP [37,38].

Before proceeding, we clarify our definition for the OSMP region and its critical temperature. This region is defined here by the situation where the population of a particular orbital (orbital three) converges to $\langle \hat{n}_3 \rangle = 1$ while a gap simultaneously opens in the density of states for this orbital. While this is a sound operative definition of our purpose, there are subtleties that must be addressed as a warning to the reader. In the context of DMFT, investigations of multiorbital models [17,29] in the plane defined by temperature T and coupling strength U/W (W is the bandwidth) show that there is an analytic connection between the Mott insulating side of a line of first order transitions and the weak coupling metallic side. The line of first-order transitions survives the introduction of temperature, but it has an end point at a finite T in analogy to the gas/liquid transition. For example, in the analysis of the localized orbital reported in Ref. [17], the quasiparticle weight Z is claimed to be nonzero at finite T on the insulating side (although it is extremely small at low temperatures). We believe that Z being zero or very small is similar to the condition that our localized orbital's population is equal to or very close to one. As a consequence, what we have defined as a transition towards an OSMP may in fact be a region where $\langle \hat{n}_3 \rangle \approx 1$ but not exactly 1. If this is the case, then our critical temperature is in reality a very sharp crossover towards a region that only reaches true OSMP characteristics at $T = 0$ (or at the much lower temperature where magnetic block correlations develop). Note that DMFT is valid in infinite dimension, while our problem is in the opposite limit, so these arguments are all qualitative at best. In spite of these subtleties, we will refer to the region below our critical temperature defined by $\langle \hat{n}_3 \rangle$ converging to 1 as an OSMP for simplicity, with the caveat that exact OSMP characteristics may be reachable only at lower T.

II. METHODS

A. Model Hamiltonian

We study a simplified three-orbital model defined on a 1D chain as introduced in Ref. [37]. This model displays a rich variety of phases including block ferromagnetism, antiferromagnetism, Mott insulting phases, metallic and band insulating phases, and several distinct OSMPs [37–39]. The Hamiltonian is $H = H_0 + H_{\text{int}}$, where

$$H_0 = -\sum_{\substack{\langle i,j \rangle \\ \sigma,\gamma,\gamma'}} t_{\gamma\gamma'} c^{\dagger}_{i,\gamma,\sigma} c_{j,\gamma',\sigma} + \sum_{i,\sigma,\gamma} (\Delta_\gamma - \mu) \hat{n}_{i,\gamma,\sigma} \quad (1)$$

contains the noninteracting terms of H, and

$$H_{\text{int}} = U \sum_{i,\gamma} \hat{n}_{i,\gamma,\uparrow} \hat{n}_{i,\gamma,\downarrow} + \left(U' - \frac{J}{2}\right) \sum_{\substack{i,\sigma,\sigma' \\ \gamma < \gamma'}} \hat{n}_{i,\gamma,\sigma} \hat{n}_{i,\gamma',\sigma'} + J \sum_{i,\gamma<\gamma'} S^{z}_{i,\gamma} S^{z}_{i,\gamma'} \quad (2)$$

contains the on-site Hubbard and Hund's interaction terms. Here, $\langle \dots \rangle$ denotes a sum over nearest neighbors, $c^{\dagger}_{i,\gamma,\sigma}(c_{i,\gamma,\sigma})$ creates (annihilates) a spin σ electron in orbital $\gamma = 1,2,3$ on site i, Δ_γ are the on-site energies for each orbital, $S^{z}_{i,\gamma}$ is the z component of the spin operator $\mathbf{S}_{i,\gamma}$, and $\hat{n}_{i,\gamma,\sigma} = c^{\dagger}_{i,\gamma,\sigma} c_{i,\gamma,\sigma}$ is the particle number operator.

Note that in Eq. (2) we have neglected the pair-hopping and spin-flip terms of the interaction. These terms can have an important influence on the details of the OSMP in higher dimensions. In the context of the current model, however, a previous DMRG [39] study found that these terms only alter the location of the phase boundaries and do not qualitatively change the nature of the underlying phases. Since our focus here is on the nonlocal correlations associated with these phases, rather than subtle issues regarding their boundaries, we neglect the spin-flip and pair hopping terms in order to manage the fermion sign problem in our DQMC calculations. These terms are also neglected in our DMRG calculations to facilitate more meaningful comparisons between the two techniques.

Following Ref. [37], we set $t_{11} = t_{22} = -0.5$, $t_{33} = -0.15$, $t_{13} = t_{23} = 0.1$, $t_{12} = 0$, $\Delta_1 = -0.1$, $\Delta_2 = 0$, and $\Delta_3 = 0.8$ in units of eV while the chemical potential μ is adjusted to obtain the desired filling. These parameters produce a noninteracting band structure analogous to the iron-based superconductors, with two holelike bands centered at $k = 0$ and an electronlike band centered at $k = \pi/a$, where a is the lattice constant, as shown in Fig. 1. Due to the weak interorbital hopping, each of the bands is primarily derived from a single orbital, as indicated by the line thickness and colors in Fig. 1. One can therefore (loosely) regard the orbital character as an indicator of the band in this model. For example, the topmost band is primarily composed of orbital $\gamma = 3$. The total bandwidth of the noninteracting model is $W = 4.9|t_{11}| = 2.45$ eV. This will serve as our unit of energy. We further set $a = 1$ as our unit of length. The interaction parameters are fixed to $U' = U - 2J$, $J = U/4$, while U is varied. This parameter regime results in a robust OSMP for intermediate values of U [37–39], which is our focus here.

B. DQMC and DMRG calculations

The model is studied using nonperturbative DQMC and DMRG methods. The details of these techniques can be found in Refs. [46–48] (DQMC) and Refs. [49] and [50] (DMRG). These approaches are complementary to one another; DMRG works in the canonical ensemble and provides access to the ground state properties of the system while DQMC works in the grand canonical ensemble and provides access to finite temperatures and fluctuations in particle number. Both methods are capable of treating large cluster sizes such that

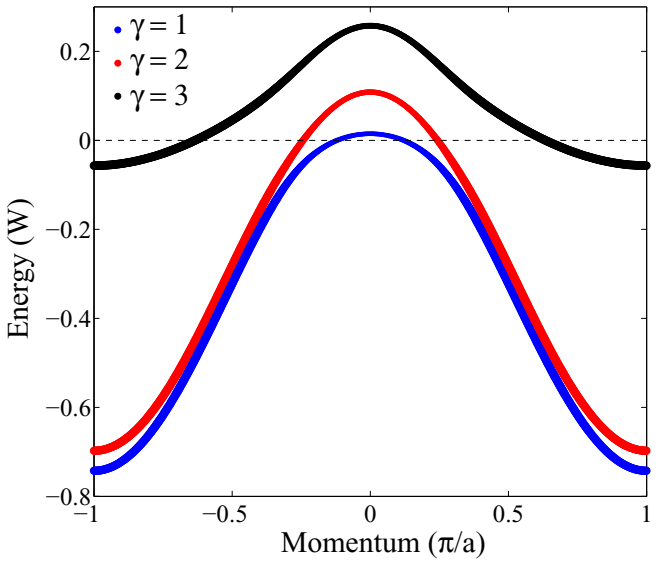

FIG. 1. Fat band plot of the noninteracting band structure at a total filling of $\langle \hat{n} \rangle = 4$, where the thickness of the lines indicates the majority orbital content of the band. The topmost band has the narrowest bandwidth and is primarily of orbital 3 character. The lower two bands disperse over a much larger energy range and are primarily composed of orbitals 1 and 2, respectively.

nonlocal correlations can be captured without approximation for the specified Hamiltonian.

The primary drawback to DQMC is the fermion sign problem [51,52], which typically limits the range of accessible temperatures for many models. Indeed, when the spin-flip and pair hopping terms of the Hund's interaction are included in the Hamiltonian, we find that the model has a prohibitive sign problem. But when these terms are neglected the corresponding sign problem becomes very mild [39], even in comparison to similar simplified multiorbital models in 2D [48,53]. Given that these terms do not qualitatively affect the phase diagram [39] for the current model, we have neglected them here. This has allowed us to study clusters of up to $L = 24$ sites in length ($3L$ orbitals in total) down to temperatures as low as $\beta = 74/W$ [39]. At this low of a temperature we begin to see the onset of magnetic correlations in our cluster; however, as we will show, the OSMP forms at a much higher temperature. Since the latter phase is our focus here, we primarily show DQMC results for $\beta \leqslant 19.6/W$ throughout. (Since our DQMC calculations find no indications of magnetism at the elevated temperatures considered here, we will not show results for the magnetic structure factor. An interested reader is directed to Ref. [39] for an indication of the magnetic correlations found at much lower temperatures.) In all cases shown here, the average value of the fermion sign is greater than 0.87 ± 0.01. Unless otherwise stated, all of our DQMC results were obtained on an $L = 24$ site cluster with periodic boundary conditions and for an average filling of $\langle \hat{n} \rangle = 4$ electrons, which corresponds to 2/3 filling.

DQMC provides direct access to various quantities defined in the imaginary time τ or Matsubara frequency $i\omega_n$ axes. In Sec. III D we will examine the spectral properties of our model, which requires an analytic continuation to the real frequency axis. This was accomplished using the method of maximum entropy [54], as implemented in Ref. [55].

Our DMRG results were obtained on variable length chains with open boundary conditions. The chemical potential term in Eq. (1) is dropped for these calculations. In all of the DMRG calculations the truncation tolerance is between 10^{-5} and 10^{-7}. We performed three to five full sweeps of finite DMRG algorithm and used 300 states for calculating both the ground state and the spectral function. Once the ground state is obtained using the standard DMRG algorithm, we computed the spectral function using the correction vector targeting in Krylov space [56,57], with a broadening of $\eta = 0.001$ eV.

III. RESULTS

A. Self-energies in the OSMP

We begin by examining some of the standard metrics for the formation of an OSMP, namely the average filling per orbital and the quasiparticle residue $Z_\gamma(k, i\omega_n)$. DQMC results for $\langle \hat{n} \rangle = 4$ and $U/W = 0.8$ are summarized in Fig. 2. The temperature dependence of the individual orbital occupations $\langle \hat{n}_\gamma \rangle$, plotted in Fig. 2(a), has the standard indications of the formation of an OSMP: at high temperature (small β) we see noninteger fillings for all three orbitals. As the temperature is lowered (large β), however, orbitals one and two smoothly approach fillings of $\sim$1.53 and $\sim$1.47, respectively, while orbital three approaches an integer value of 1. In many studies the "stiffness" of orbital three's integer occupation is taken as an indication of an OSMP [37,38], where this orbital has undergone a transition to a Mott insulating state while remaining orbitals host itinerant electrons. Indeed, for $U/W = 0.8$ and at low temperature, the integer filling observed in orbital three is robust against changes in the chemical potential and interaction strength U (see Refs. [37–39]). This indicates that this integer filling is indeed driven by the interaction and is not a simple coincidence of the noninteracting band parameters. However, as we will show, this does not always correspond to an OSMP. For $U/W = 0.8$ the two fractionally filled orbitals are in fact itinerant, but for larger values of U/W these same orbitals retain a fractional filling but are driven into an insulating state by the onset of orbital ordering in these two orbitals.

The mixed itinerant/localized nature of the OSMP at $U/W = 0.8$ is reflected in the momentum dependence of quasiparticle residue $Z_\gamma(k, i\pi/\beta)$ and the orbitally resolved normalized self-energies $R(k) = \mathrm{Im}\Sigma_\gamma(k, i\pi/\beta)/\mathrm{Im}\Sigma_\gamma(0, i\pi/\beta)$, plotted in Figs. 2(c) and 2(d), respectively, for $\omega_n = \pi/\beta$. The self-energy is extracted from the dressed Green's function using Dyson's equation

$$\hat{G}^{-1}(k, i\omega_n) = \hat{G}_0^{-1}(k, i\omega_n) - \hat{\Sigma}(k, i\omega_n), \tag{3}$$

where the $\hat{G}$ notation denotes a matrix in orbital space, $\hat{G}_0(k, i\omega_n) = [i\omega_n \hat{I} - \hat{H}_0(k)]^{-1}$ is the noninteracting Green's function, and $\hat{H}_0(k)$ is the Fourier transform of the noninteracting Hamiltonian defined in orbital space. The quasiparticle residue is obtained from the diagonal part of the self-energy

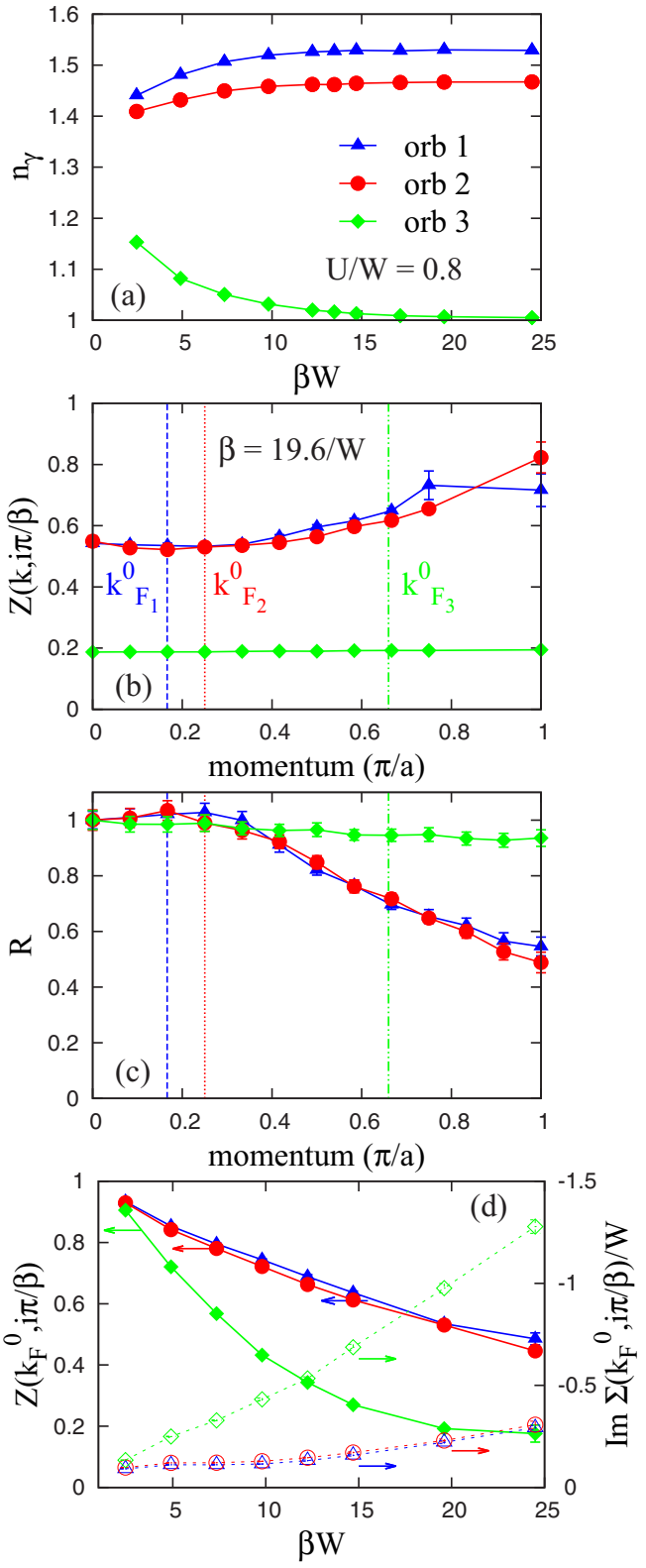

FIG. 2. Orbitally resolved electronic properties for $U/W = 0.8$ ($W = 2.45$ eV) at different temperatures. (a) The temperature dependence of orbital occupations. (b) The orbital resolved quasiparticle residue $Z_\gamma(k,i\pi/\beta)$ at an inverse temperature $\beta = 19.6/W$. (c) The normalized electron self energies $\mathrm{Im}\Sigma_\gamma(k,i\pi/\beta)$ at $\omega_n = \pi/\beta$ as a function of momentum. Each curve is normalized by its $k = 0$ value to highlight the overall momentum dependence. The scale is determined by $\mathrm{Im}\Sigma_\gamma(0,i\pi/\beta) = -0.53$, -0.57, and -2.53 for $\gamma = 1,2,3$, respectively, and in units of the bandwidth W. The blue, red, and green dash lines in (b) and (c) correspond to the bare Fermi momentum of the noninteracting bands. Panel (d) shows orbitally resolved quasiparticle residues $Z_\gamma(k_F^0,i\pi/\beta)$ and self-energies $\mathrm{Im}\Sigma_\gamma(k_F^0,i\pi/\beta)$ at Fermi momentum as a function of temperature. In each panel, error bars smaller than the marker size have been suppressed for clarity.

using the identity

$$\hat{Z}(k,i\pi/\beta) = \left(\hat{I} - \frac{\mathrm{Im}\hat{\Sigma}(k,i\pi/\beta)}{\pi/\beta}\right)^{-1}, \tag{4}$$

where $\hat{I}$ is a 3×3 unit matrix.

As can be seen from Fig. 2(c), the self-energies for each orbital have a sizable k dependence at this temperature. (We have normalized the self-energy by its value at $k = 0$ in order to highlight the overall momentum dependence. The magnitude of $\mathrm{Im}\Sigma_\gamma(0,i\pi/\beta)$ is given in the figure caption.) In the case of orbitals one and two, the magnitude of the self-energy varies by nearly 50% throughout the Brillouin zone. In contrast, the momentum dependence of $\Sigma_3(k,i\pi/\beta)$ for orbital three is much weaker, varying by only 5% –10% and reflecting the localized nature of the carriers in these orbitals. Similarly, the quasiparticle residue for orbital three is essentially momentum independent, while it increases for the two itinerant orbitals as k tracks towards the zone boundary. The k dependence at the remaining Matsubara frequencies accessible to our simulations (not shown) exhibits a similar trend, with orbitals one and two having a strong k dependence while orbital three is nearly momentum independent at each ω_n.

The momentum dependence shown in Fig. 2 indicates that the local self-energy approximation introduced by DMFT may miss quantitative aspects of the electronic correlations in the OSMP with mixed itinerant and local characteristics. It should be noted that our results have been obtained in 1D, which is the worst case situation for DMFT [58]. It is expected that the local approximation will perform better in higher dimensions, since DMFT becomes exact in the limit of infinite dimensions; however, it is unclear how well the method will capture similar nonlocal correlations in two dimensions relevant for the Fe-based superconductors. A recent study [16] has argued that the local approximation is quite accurate for parameters relevant to the iron-based superconductors, but it remains to be seen if this will remain true for all parameter regimes or when longer range fluctuations are included. Our results further highlight the need for the continued development of numerical methods capable of handling the strong Hubbard and Hund's interactions in intermediate dimensions and on extended clusters.

Figure 2(d) examines the temperature dependence of $Z(k_F^0,\frac{i\pi}{\beta})$ and $\mathrm{Im}\Sigma(k_F^0,\frac{i\pi}{\beta})$ at the Fermi momenta k_F^0 of the noninteracting system. [These are indicated by the dashed lines in 2(b) and 2(c).] Here, we find indications of anomalous behavior for the itinerant electrons, where the quasiparticle residues of all three orbitals decrease with temperature. This is accompanied by an increase in $\mathrm{Im}\Sigma(k_F,\frac{i\pi}{\beta})$ as T is lowered. This is perhaps expected for orbital three, as Z ($\mathrm{Im}\Sigma$) for the localized orbital should decrease (increase) as this orbital

becomes more localized. For the itinerant orbitals, however, one would naively expect the self-energy to decrease as temperature is lowered, which is opposite to what is observed. We believe that this is due to the Hund's interaction between the itinerant electrons and the localized spins on orbital three. At this temperature we find no evidence of a magnetic ordering in our model [39], despite the fact that a local moment has clearly formed in the OSMP. This means that the orientation of the local moment is random and fluctuating at these temperatures. This produces a fluctuating potential acting on the itinerant electrons via the Hund's coupling, thus generating a residual scattering mechanism at low temperatures that reduces the quasiparticle residue and increases the self-energy.

B. Momentum and temperature dependence of the spectral weight

Next, we turn to the momentum dependence of the spectral weight for the three orbitals in the vicinity of the Fermi level. This can be estimated directly from the imaginary time Green's function using the relationship [59]

$$\beta G(k,\tau=\beta/2)=\frac{\beta}{2}\int d\omega\frac{A(k,\omega)}{\cosh\left(\frac{\beta\omega}{2}\right)},$$

where $A(k,\omega)$ is the single-particle spectral function. At low temperature, the function $\frac{\beta}{2}\cosh^{-1}(\frac{\beta\omega}{2})$ is sharply peaked around $\omega=E_F=0$. The quantity $\beta G(k,\tau=\beta/2)$ therefore provides a measure of the spectral weight at momentum k, integrated within a window of a few β^{-1} of the Fermi level. Using this relationship we do not have to perform the extra step of analytically continuing the data to the real frequency axis.

Figures 3(a)–3(c) summarize $\beta G(k,\beta/2)$ for $U/W=0.1$, $U/W=0.8$, and $U/W=2$, respectively. The results in the weak coupling limit [$U/W=0.1$, Fig. 3(a)] are consistent with that of a fully itinerant system: all three orbitals have a maximal spectral weight at a momentum point very close to the Fermi momenta of the noninteracting system (indicated by the dashed lines). This is exactly the behavior one expects for a well-defined quasiparticle band dispersing through E_F, where the peak in the spectral weight occurs at k_F. The proximity of the peaks in $\beta G(k,\beta/2)$ to the noninteracting values of k_F indicates that the Fermi surface is only weakly shifted for this value of the interaction parameters. However, as we will show in Sec. III C, these shifts are band dependent.

In the intermediate coupling regime [$U/W=0.8$, Fig. 3(b)], where the OSMP has formed, we again see both localized and itinerant characteristics. The spectral weight of the localized orbital is small and independent of momentum, as expected for the formation of a localized Mott state. Conversely, the spectral weight of the remaining orbitals still exhibits a momentum dependence characteristic of dispersive bands. Despite this, the total spectral weight is decreased, indicating that spectral weight has been transferred to higher binding energies by the Hubbard and Hund's interactions. This is also reflected in the position of the maximum spectral weight, which has shifted to a slightly larger k value due to a renormalization of the Fermi surface by the interactions. We also observe that the spectral weight at the zone boundary increases relative to the zone center, consistent with a flattening

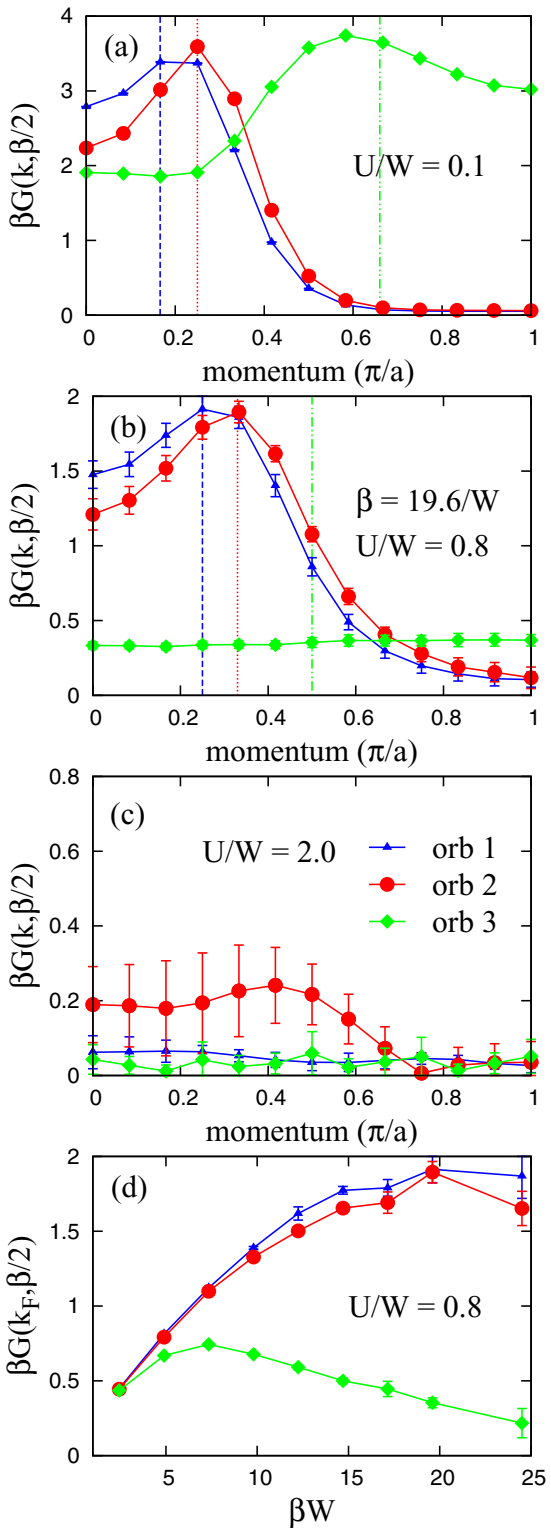

FIG. 3. Momentum dependence of Green functions $G(k,\tau=\beta/2)$ for (a) $U/W=0.1$, (b) 0.8, and (c) 2.0. The inverse temperature in all three cases is $\beta=19.6/W$. The blue, red, and green dash lines in each panel indicate the Fermi momentum of the three noninteracting bands. (d) $G(k_F,\tau=\beta/2)$ as a function of inverse temperatures β for the OSMP $U/W=0.8$. Error bars smaller than the marker size have been suppressed for clarity.

of the bands and a broadening of the spectral function with increasing U. (This will be confirmed shortly when we examine the spectral functions directly.) A similar transfer of spectral weight was observed in a two-dimensional cluster DMFT study [35].

The temperature evolution of spectral weight $\beta G(k_F,\beta/2)$ at the Fermi momentum for the OSMP ($U/W = 0.8$) is shown in Fig. 3(d). In a metallic system one generally expects the spectral weight at the Fermi level to increase as the temperature is decreased. Initially, this is what is observed for all three orbitals; however, the spectral weight for orbital three reaches a maximum around $\beta = 7.5/W$ before decreasing as the temperature is lowered further and the OSMP gap forms on this orbital. Conversely, the spectral weight of the itinerant orbitals continues to rise until saturating at $\beta/W \approx 15$. This saturation is again due to the presence of a residual scattering channel, which we associate with the fluctuating localized spins present on the localized orbital three.

The $U/W = 0.8$ results confirm the mixed itinerant/local character of the model at intermediate coupling. When the value of U is further increased, we find that all three bands become localized while maintaining partial occupancies for each band. To demonstrate this, Fig. 3(c) shows results for $U/W = 2$. In this case, the orbital occupations for the three orbitals are $\langle \hat{n}_1 \rangle = 1.55$, $\langle \hat{n}_2 \rangle = 1.44$, and $\langle \hat{n}_3 \rangle = 1$, which are similar to those obtained at $U/W = 0.8$. At face value one might therefore conclude that the system is in an OSMP [37,39]; however, an examination of the spectral weight reveals that the system is in fact insulating. As can be seen in Fig. 3(c), at $U/W = 2$ and $\beta = 19.6/W$, $\beta G(k,\beta/2)$ is nearly momentum independent and the total spectral weight of all three orbitals has significantly decreased (note the change in scale of the y axis). This behavior is indicative of the formation of a charge gap throughout the Brillouin zone. The ultimate origin of this insulating behavior is the formation of a long-range orbital ordering, as we will show in Sec. III D.

C. Band-dependent Fermi surface renormalization

It is now well known that *ab initio* band structure calculations based on density functional theory (DFT) do not describe the electronic structure of the iron based superconductors as measured in ARPES experiments. (For a recent review, see Ref. [4].) Generally speaking, the calculated band structure usually needs to be rescaled by an overall factor, which is attributed to reduction in bandwidth driven by electronic correlations. In addition, the size of the Fermi surfaces is often overestimated by DFT in comparison to measurements. A prominent example of this is LiFeAs [60], where the innermost hole pocket realized in nature is substantially smaller than the one predicted by DFT [61,62]. In order to correct this, the electron and hole bands need to be shifted apart [4], which requires a momentum-dependent self-energy correction.

We examine this issue within our model in Fig. 4, which plots the expectation value of the orbitally resolved number operator in momentum space $n_\gamma(k) = \frac{1}{2}\sum_\sigma \langle c^\dagger_{k,\gamma,\sigma} c_{k,\gamma,\sigma} \rangle$ for various values of the interaction strength. In the noninteracting limit, and in a single-band case, this quantity is equal to the Fermi-Dirac distribution and the location of the leading edge corresponds to k_F. In a multiband system the mixing of the

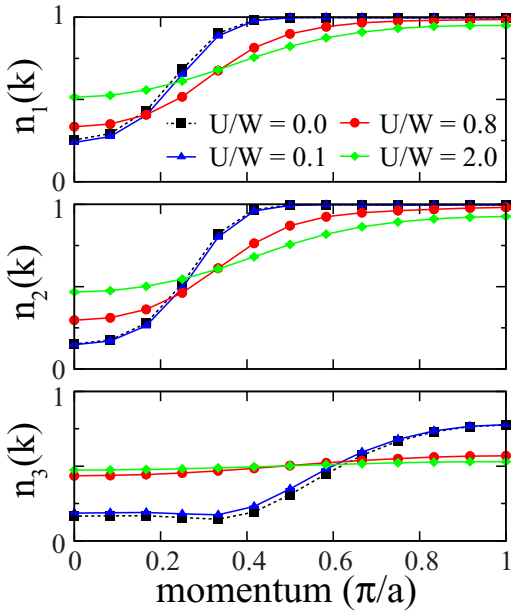

FIG. 4. Momentum dependence of the number operator $n_\gamma(k) = \frac{1}{2}\sum_\sigma \langle c^\dagger_{k,\gamma,\sigma} c_{k,\gamma,\sigma} \rangle$ for each band. Results are shown for the noninteracting case $U = 0$ (black dashed, □), $U/W = 0.1$ (blue solid, △), $U/W = 0.8$ (red solid ○), and $U/W = 2$ (green solid ◇) and at an inverse temperature of $\beta = 19.6/W$.

orbital character complicates this picture; however, in our model the leading edge still corresponds to k_F due to the weak hybridization between orbitals. In the weak coupling case ($U/W = 0.1$) we observe a small shift in the position of the leading edge. Within error bars, the curve $n_1(k)$ and $n_2(k)$ shift to slightly larger momenta while $n_3(k)$ shifts towards smaller momenta. This indicates that the size of the Fermi surfaces are increasing and the electronlike and holelike bands are shifted towards one another by the interactions. This trend continues as U/W is increased to 0.8; however, in this case the electronlike band is significantly smeared out due to the formation of the OSMP.

We note that the direction of the band shifts is reversed from what is generally required for the two-dimensional iron-based superconductors, where the calculated holelike Fermi surfaces generally need to be shrunk relative to the electronlike Fermi surfaces. We attribute this to differences in the underlying tight-binding model and differences in dimensionality. In this light, it would be interesting to compare the ARPES observed band structures in the quasi-one-dimensional pnictides against the predictions of our model and DFT calculations [42]. Nevertheless, our results do show that nonlocal correlations arising from a local interaction can produce relative shifts of the electronlike and holelike bands in a multiorbital system.

D. Spectral properties

1. *Intermediate coupling $U/W = 0.8$*

We now examine the spectral properties of the model, beginning with the OSMP. Figure 5(a) shows the temperature evolution of the total density of states (DOS) at $U/W = 0.8$, which is obtained from the trace of the orbital-resolved

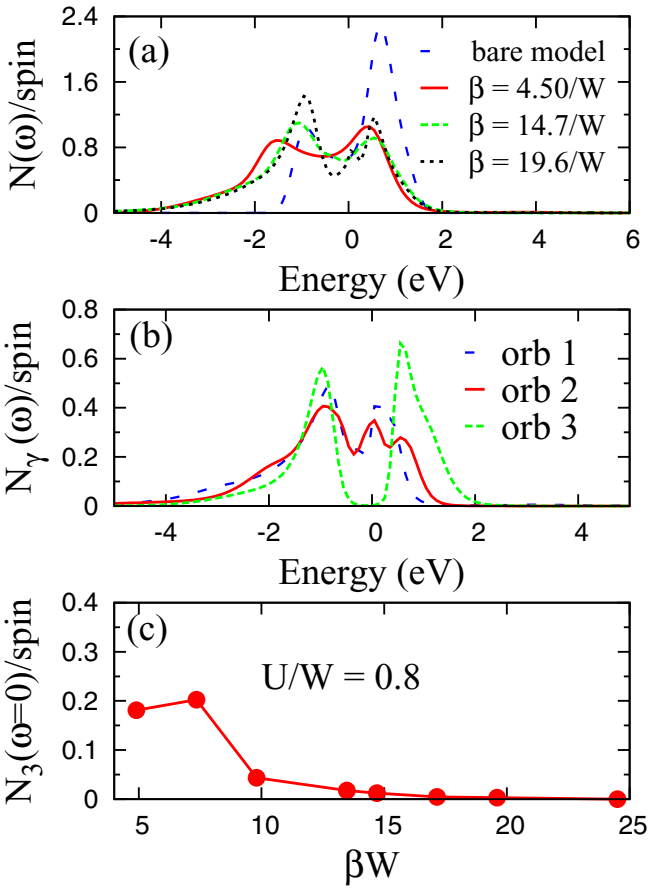

FIG. 5. (a) Density of states at different temperatures. (b) The orbitally resolved density of states for each orbital at an inverse temperature $\beta = 19.6/W$. (c) The density of states at the Fermi surface of the orbital 3 as a function of inverse temperatures β. The Coulomb interaction strength is $U/W = 0.8$ in all three graphs.

spectral function $N(\omega) = -\frac{1}{\pi L}\sum_{k,\gamma} \mathrm{Im}\hat{G}_{\gamma\gamma}(k,\omega + \mathrm{i}\delta)$. In the noninteracting limit [the long-dashed (blue) curve], the DOS has a double peak structure, where the lower (upper) peak corresponds to the bands derived from orbitals one and two (orbital three). The overall structure of the DOS in the interacting case is similar at high temperatures, but some spectral weight is transferred to a broad incoherent tail extending to lower energies. As the temperature is decreased, the peak on the occupied side shifts towards the Fermi level and sharpens. At the same time, a small amount of spectral weight is transferred from the vicinity of the Fermi level into this peak. The appearance of this apparent "pseudogap" is a direct consequence of the OSMP forming on orbital three, which is easily confirmed by examining the orbital-resolved DOS $N_\gamma(\omega) = -\frac{1}{\pi L}\sum_k \mathrm{Im}\hat{G}_{\gamma,\gamma}(k,\omega)$ shown in Fig. 5(b). As can be clearly seen, orbitals one and two have a finite DOS at $\omega = 0$, while orbital three is fully gapped at low temperature.

We also begin to see the formation of an additional peak near the Fermi level at the lowest temperature we examined ($\beta = 19.6/W$). This feature is more clearly seen in the orbital-resolved DOS [Fig. 5(b)], where it is found to originate from the itinerant orbitals. This peak is due to a hybridization between the itinerant and localized orbitals, which is observable in the k-resolved spectral functions (see Fig. 6).

The relevant temperature scale for the formation of the OSMP can be estimated by tracking $N_3(0)$ as a function of temperature, as shown in Fig. 5(c). Here, a continuous suppression of $N_3(0)$ is observed, with the value reaching zero at $\beta \approx 20/W$. The rate at which $N_3(0)$ decreases also undergoes a distinct change at $\beta \approx 7.5/W$, which coincides with the temperature at which the spectral weight for this orbital at k_F is largest [see Fig. 3(d)]. We interpret this to mean that the Mott gap on orbital three begins to form at $\beta W \approx 10$ (on the $L = 24$ site lattice), growing continuously from zero as the temperature is lowered. In this case, the finite spectral weight between $\beta W = 10 - 20$ is due to thermal broadening across this gap. Since we have observed similar behavior on smaller clusters with DQMC and at zero temperature using DMRG, we believe that the transition to the OSMP will survive in the thermodynamic limit; however, the gap magnitude has some finite size dependence.

The extended length of our 1D cluster grants us access to the momentum dependence of the spectral function, which is shown in Fig. 6. The top row of Fig. 6 shows the results in the OSMP with $U/W = 0.8$ and $\beta = 19.6/W$, which is the same parameter set used in Fig. 5. The total spectral function $A(k,\omega) = -\frac{1}{\pi}\mathrm{Tr}[\mathrm{Im}\hat{G}(k,\omega)]$ is shown in Fig. 6(a) and the orbital-resolved components $A_\gamma(k,\omega) = -\frac{1}{\pi}\mathrm{Im}\hat{G}_{\gamma\gamma}(k,\omega)$ are shown in Figs. 6(b)–6(d), as indicated. The lower row of Fig. 6 shows similar results obtained for $U/W = 2$ and $L = 8$. (In this case a smaller cluster is sufficient due to the localized nature of the band dispersions.)

The results in the OSMP with $U/W = 0.8$ reveal localized and itinerant characteristics that are consistent with the spectral weight analysis presented earlier. The itinerant orbitals primarily contribute to dispersing bands that track through E_F ($\omega = 0$), while orbital three has split into two relatively dispersionless upper and lower Hubbard bands above and below E_F. At first glance, these Hubbard bands appear to be sharper than the corresponding Hubbard bands in the single-band Hubbard model; however, an examination of the DOS [Fig. 5(b)] reveals that they are spread out over an energy interval that is larger than the noninteracting bandwidth of the topmost band ($W_3 \sim 0.3W \sim 0.735$ eV). In addition to the formation of the Hubbard bands for orbital 3, we also observe two additional effects. The first is an expected narrowing of the bandwidth of the itinerant bands. For this parameter set we obtain $W_1 \sim 1.7$ and $W_2 \sim 1.65$ eV for orbitals one and two, respectively, which should be compared to the noninteracting values of 1.88 and 1.97 eV. The second is the aforementioned hybridization and level repulsion between the itinerant and localized orbitals. This is manifest in the spectral function as a slight "buckling" of orbital three's upper Hubbard band near $k = 0$, and the tracking of orbital one's spectral weight along E_F near $k = \pm\pi/2a$. It is this trailing intensity that forms the peak observed in the DOS just above the Fermi level at low temperatures.

2. *Strong coupling $U/W = 2$*

The spectral properties of the model are very different when the Hubbard interaction is increased to $U/W = 2$.

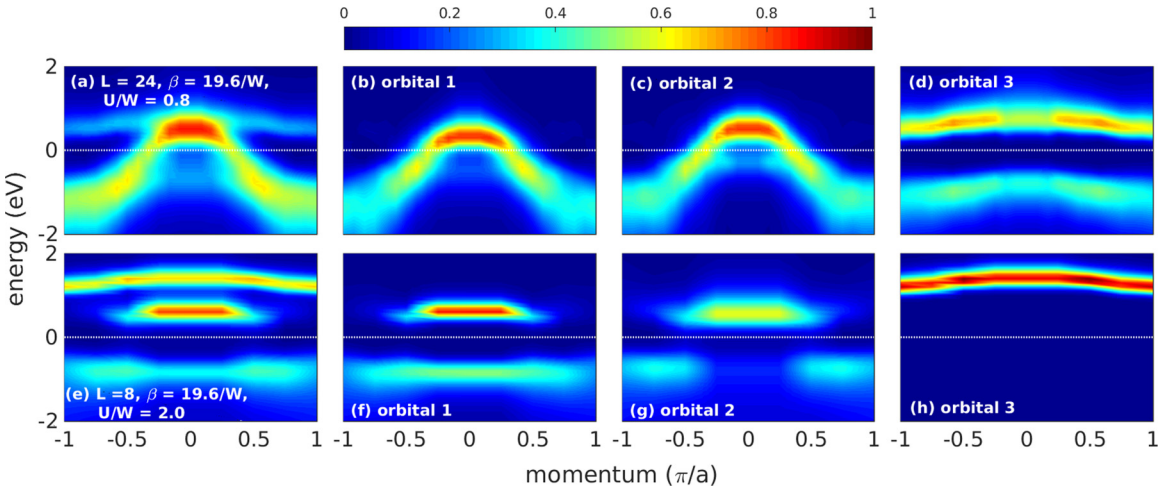

FIG. 6. (a) Spectral function for $U/W = 0.8$. (b), (c), and (d) are the orbital 1, 2, and 3 parts of the spectral function in (a), respectively. (e) The spectral function for $U/W = 2$. (f), (g), and (h) are the orbital 1, 2, and 3 parts of the spectral function in (e), respectively. The dash white line labels the Fermi surface. The inverse temperature is set as $\beta = 19.6/W$. Results were obtained with maximum entropy DQMC.

In this case, the total spectral function [Fig. 6(e)] and its orbitally resolved components [Figs. 6(f)–6(h)] all split into relatively flat Hubbard-like bands above and below E_F. (In the case of orbital three, the lower band below E_F has been pushed outside of the energy range shown in the figure.) For this value of the interaction strength there is no spectral weight at the Fermi level, and the system is insulating even though orbitals one and two have an average 1.55 and 1.44 electrons/orbital, respectively. (These values are obtained both from the measured equal time orbital occupancies, and from integrating the total spectral weight above and below E_F.)

The imaginary axis spectral weight analysis [Fig. 3(c)] and the spectral function analysis (Fig. 6) both indicate that for $U/W = 2$ the model is an insulator. The origin of this behavior is the combined action of the Hund's coupling and the onset of an orbital ordering of the itinerant orbitals. All indications show that orbital three has already undergone an orbital selective Mott phase transition (OSMT) when $U/W = 2$. This has the effect of localizing one electron per site within this subset of orbitals while leaving three additional electrons to be distributed among the remaining two itinerant orbitals. A sizable Hund's coupling will decouple the individual orbitals when the crystal field splittings are smaller than the bandwidth of the material [22]. This is precisely the situation at hand, and thus the remaining nominally itinerant orbitals are decoupled from the localized orbital by the large $J = U/4$. This results in an effective nearly degenerate two-band system with (nearly) three-quarters filling. This is a special case for the two-orbital Hubbard model, which is prone to orbital ordering in one and two dimensions [28,63,64].

The situation is sketched in Fig. 7. Assuming ferromagnetic nearest neighbor correlations for orbital three, we have a low-energy ground state configuration as shown in the left side of Fig. 7(a). Here, orbitals one and two adopt alternating double occupations in order to maximize their delocalization energy through virtual hopping processes. This results in near-neighbor orbital correlations. Subsequent charge fluctuations such as the one shown in the right side of the Fig. 7(a) cost a potential energy PE $\sim U' - J = W/2$. This is compensated for by a kinetic energy gain KE $\sim 4t_{11} \sim 4W/4.9$. The ratio between these competing energy scales is $\sim 5/8$, suggesting that charge fluctuations are strongly suppressed by the strong electronic correlations in this subsystem. Note that the situation is worse for antiferromagnetic nearest neighbor correlations in orbital three. The energy cost in this case increases to $\sim U'$, as shown in Fig. 7(b). Thus both ferro- and antiferromagnetic correlations in orbital three will suppress charge fluctuations and promote orbital ordering. Since the type of magnetic correlations does not matter, such orbital ordering tendencies can be expected in the paramagnetic phases, provided the localized moments have formed in orbital three. This picture is then consistent with insulating behavior (and short-range orbital ordering tendencies; see below) at high temperatures, where no magnetic correlations are observed.

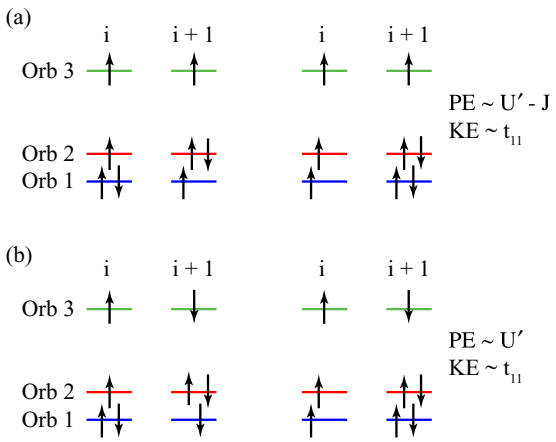

FIG. 7. Cartoon sketch of the relevant charge fluctuation processes leading to the insulating state when $U/W = 2$ assuming (a) ferromagnetic and (b) antiferromagnetic nearest neighbor correlations within the orbital that has undergone the orbital selective Mott transition (orbital three).

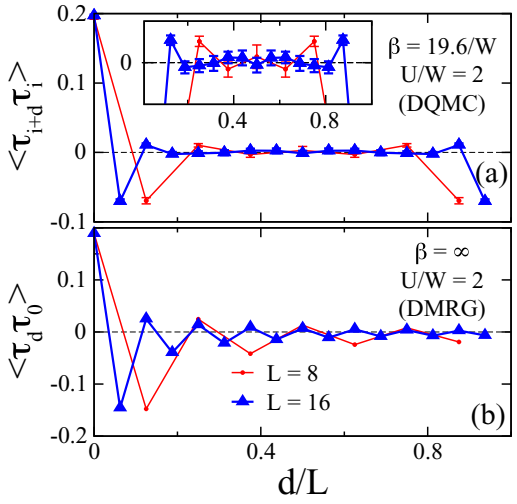

FIG. 8. Results for the orbital correlation function for the system in the strong coupling case $U/W = 2$. Results are obtained at (a) finite temperature using DQMC and (b) $T = 0$ ($\beta = \infty$) using DMRG. In both cases, results are shown on $L = 8$ (red dots) and $L = 16$ (blue triangles) chains. The DQMC results were obtained on a chain with periodic boundary conditions. The DMRG results were obtained on a chain with open boundary conditions.

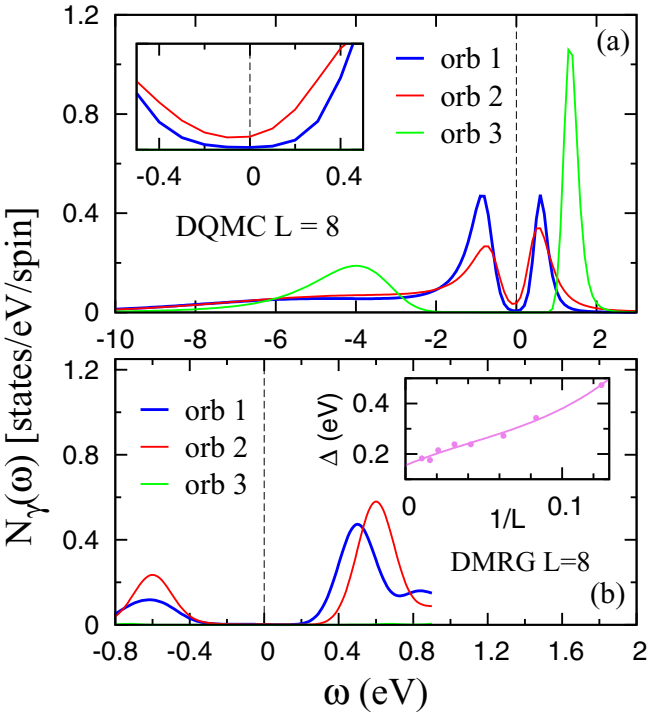

FIG. 9. Results for the orbitally resolved density of states for each orbital obtained for $U/W = 2$ and on $L = 8$ site chains. Panel (a) shows DQMC results at $\beta = 19.6/W$ and the inset zooms in to energy around Fermi surface. Panel (b) shows DMRG results for the same conditions but at zero temperature ($\beta = \infty$). The inset plots a finite size scaling analysis of the charge gap obtained within DMRG (see text). The dash line in both panels indicates the Fermi energy.

We verify this picture explicitly in Fig. 8, which plots the equal-time orbital correlation function $\langle \hat{\tau}_{i+d} \hat{\tau}_i \rangle$, with $\hat{\tau}_i = (\hat{n}_{i,2} - \hat{n}_{i,1})$. Here, results are shown for finite temperature DQMC calculations [Fig. 8(a)] and zero temperature DMRG calculations [Fig. 8(b)] and with $U/W = 2$ in both cases. The "long-range" (with respect to the cluster size) anti-ferro-orbital correlation is clear in the zero temperature results obtained on $L = 8$ and $L = 16$ chains. At finite temperatures ($\beta = 19.6/W$) we find that the orbital correlations are suppressed at long distances, but local anti-ferro-orbital correlation remains on shorter length scales. These combined results demonstrate the presence of short-range orbital correlations at higher temperatures, which grow in length as the temperature is decreased. The corresponding orbitally resolved DOS are plotted in Fig. 9 for both cases. Both methods predict that the system is insulating, with a charge gap width on orbitals one and two of about 0.5 eV (estimated from half the peak-to-peak distance in the DOS). The presence of a gap at finite temperature also confirms that the short range orbital correlations are sufficient to open a gap in the spectral function. Finally, we stress these results will survive in the thermodynamic limit $L \to \infty$. This is confirmed in the inset in Fig. 9(b), which plots the $T = 0$ gap Δ as a function of chain length L, as obtained from DMRG. In this case, computing the DOS for the longer chains is impractical. Therefore, we defined an alternative measure of the gap as $\Delta = E(N+1) + E(N-1) - 2E(N)$, where $E(N)$ is the ground state energy of the system with $N = 4L$ electrons. This definition agrees with the gap size obtained directly from the DOS that was explicitly computed for the shorter chains. Using this, we find that the DMRG gap size Δ decreases with increasing chain lengths, until reaching a value of $\sim$0.2 eV in the $L \to \infty$ limit.

IV. DISCUSSION AND SUMMARY

We have performed a momentum-resolved study of a multiorbital model defined on extended 1D chains using nonperturbative DQMC and DMRG. This has allowed us to compute the several properties of an OSMP in a momentum resolved manner without resorting to approximate methods. We find that several properties do indeed exhibit significant momentum dependencies, not be captured by local approximations introduced by DMFT; however, the 1D case we have considered represents the worst case for DMFT. In that sense our results complement existing DMFT efforts by providing analysis in a region where the method is expected to perform badly.

Our results establish the hierarchy of charge and magnetic orderings in this model. At low temperatures, our DMRG calculations (as well as those in Ref. [37]) demonstrate that orbital three is ferromagnetically ordered at $T = 0$. Contrary to this, our finite temperature DQMC calculations find no indications of any magnetic order for $\beta < 19.6/W$; the magnetic structure factor $S(q)$ is completely featureless as a function of q at these temperatures. Despite this, our finite T calculations find an orbital-selective Mott phase, as well as a fully insulating phase arising due to short-range orbital ordering, depending on the strength of the Hubbard interaction U. We therefore conclude that the charge ordering occurs before any magnetic ordering in this model.

The results shown in Figs. 2(d) and 3(d) show that orbital three in our model, which has the narrowest bandwidth, undergoes a transition to a Mott phase at $\beta W \sim 10$–15. This in combination with the lack of magnetic signal means that OSMP in this parameter regime is a true Mott phase as opposed to a Slater insulator where the insulating behavior is driven by magnetism. Our results also demonstrate that it is insufficient to identify an OSMP using the orbital occupations only in some instances. One should be particularly careful in regions of parameter space where the itinerant bands have average occupations close to special cases known for one- and two-orbital Hubbard models. In our case, the average fillings of the itinerant orbitals are $\langle \hat{n}_1 \rangle \sim 1.53$ and $\langle \hat{n}_2 \rangle \sim 1.47$, values very close to the special case of 3/4 filling in a degenerate two-band Hubbard model. At zero temperature, our DMRG results obtain fillings of 1.5 for each orbital.

The orbital correlations in Fig. 8 give some indication as to the extent of the cluster one might need to capture these effects using embedded cluster techniques. The $\beta = 19.6/W$ results shown in Fig. 8(a) indicate that the orbital correlations extend over (at least) three lattice sites within the error bars of our data, while at $T = 0$ the correlations [Fig. 8(b)] extend over the length of the cluster. Thus the low-temperature correlation length can be quite long, even in 1D. Single-site mean-field approaches cannot capture these correlations in either case. However, one might hope that DCA or cluster DMFT extensions may be able to address the short range correlations at elevated temperatures.

Finally, we discuss our results in the context of recent experimental work. ARPES results for AFe_2As_2 have found evidence that the OSMP in these materials disappears as the temperature is lowered [65]. This behavior was explained using a slave-boson approach and attributed to the reduced entropy in the metallic phase in comparison to the OSMP. Our results do not show this behavior, and the OSMP is found at low temperature. This difference may be related to the differences in the dimensionality (one vs two) or number of orbitals (three vs five) between the models, or the differences between our nonperturbative approach and other mean-field methods. This highlights the need for continued application of nonperturbative methods to tractable multiorbital Hubbard models.

ACKNOWLEDGMENTS

The authors thank G. Liu for useful discussions. S.L., Y.W., and S.J. are supported by the University of Tennessee's Science Alliance Joint Directed Research and Development (JDRD) program, a collaboration with Oak Ridge National Laboratory. N.K. and E.D. were supported by the National Science Foundation (NSF) under Grant No. DMR-1404375. Y.T. and T.A.M. acknowledge support by the Laboratory Directed Research and Development Program of Oak Ridge National Laboratory, managed by UT-Battelle, LLC, for the US Department of Energy (DOE). Part of this work was conducted at the Center for Nanophase Materials Science, sponsored by the Scientic User Facilities Division (SUFD), Basic Energy Sciences (BES), DOE, under contract with UT-Battelle. A.N. and G.A. acknowledge support by the Early Career Research program, SUFD, BES, DOE. CPU time was provided in part by resources supported by the University of Tennessee and Oak Ridge National Laboratory Joint Institute for Computational Sciences (http://www.jics.utk.edu).

[1] D. C. Johnston, The puzzle of high temperature superconductivity in layered iron pnictides and chalcogenides, Adv. Phys. **59**, 803 (2010).

[2] G. R. Stewart, Superconductivity in iron compounds, Rev. Mod. Phys. **83**, 1589 (2011).

[3] P. C. Dai, J. P. Hu, and E. Dagotto, Magnetism and its microscopic origin in iron-based high-temperature superconductors, Nat. Phys. **8**, 709 (2012).

[4] A. van Roekeghem, P. Richard, H. Ding, and S. Biermann, Spectral properties of transition metal pnictides and chalcogenides: Angle-resolved photoemission spectroscopy and dynamical mean field theory, C. R. Phys. **17**, 140 (2016).

[5] R. Yu and Q. Si, Orbital-Selective Mott Phase in Multiorbital Models for Alkaline Iron Selenides $K_{1-x}Fe_{2-y}Se_2$, Phys. Rev. Lett. **110**, 146402 (2013).

[6] L. Fanfarillo and E. Bascones, Electronic correlations in Hund metals, Phys. Rev. B **92**, 075136 (2015).

[7] Y.-Z. Zhang, H. Lee, H.-Q. Lin, C.-Q. Wu, H. O. Jeschke, and R. Valentí, General mechanism for orbital selective phase transitions, Phys. Rev. B **85**, 035123 (2012).

[8] C. Knecht, N. Blümer, and P. G. J. van Dongen, Orbital-selective Mott transitions in the anisotropic two-band Hubbard model at finite temperatures, Phys. Rev. B **72**, 081103(R) (2005).

[9] A. Liebsch, Novel Mott Transitions in a Nonisotropic Two-Band Hubbard Model, Phys. Rev. Lett. **95**, 116402 (2005).

[10] A. Georges, L. de' Medici, and J. Mravlje, Strong correlations from Hunds coupling, Annu. Rev. Condens. Matter Phys. **4**, 137 (2013).

[11] M. Ferrero, F. Becca, M. Fabrizio, and M. Capone, Dynamical behavior across the Mott transition of two bands with different bandwidths, Phys. Rev. B **72**, 205126 (2005).

[12] L. de' Medici, A. Georges, and S. Biermann, Orbital-selective Mott transition in multiband systems: Slave-spin representation and dynamical mean-field theory, Phys. Rev. B **72**, 205124 (2005).

[13] L. de' Medici, S. R. Hassan, M. Capone, and X. Dai, Orbital-Selective Mott Transition Out of Band Degeneracy Lifting, Phys. Rev. Lett. **102**, 126401 (2009).

[14] P. Werner and A. J. Millis, High-Spin to Low-Spin and Orbital Polarization Transitions in Multiorbital Mott Systems, Phys. Rev. Lett. **99**, 126405 (2007).

[15] A. Mukherjee, N. D. Patel, A. Moreo, and E. Dagotto, Orbital selective directional conductor in the two-orbital Hubbard model, Phys. Rev. B **93**, 085144 (2016).

[16] P. Sémon, K. Haule, and G. Kotliar, Validity of the local approximation in iron-pnictides and chalcogenides, arXiv:1606.03660.

[17] A. Liebsch, Single Mott transition in the multiorbital Hubbard model, Phys. Rev. B **70**, 165103 (2004).

[18] N. Lanatà, H. U. R. Strand, G. Giovannetti, B. Hellsing, L. de' Medici, and M. Capone, Orbital selectivity in Hund's

metals: The iron chalcogenides, Phys. Rev. B **87**, 045122 (2013).
[19] Z. P. Yin, K. Haule, and G. Kotliar, Kinetic frustration and the nature of the magnetic and paramagnetic states in iron pnictides and iron chalcogenides, Nat. Mater. **10**, 932 (2011).
[20] V. I. Anisimov, I. A. Nekrasov, D. E. Kondakov, T. M. Rice, and M. Sigrist, Orbital-selective Mott-insulator transition in $Ca_{2-x}Sr_xRuO_4$, Eur. Phys. J. B **25**, 191 (2002).
[21] N. Mannella, The magnetic moment enigma in Fe-based high temperature superconductors, J. Phys.: Condens. Matter **26**, 473202 (2014).
[22] L. de' Medici, G. Giovannetti, and M. Capone, Selective Mott Physics as a Key to Iron Superconductors, Phys. Rev. Lett. **112**, 177001 (2014).
[23] For a recent review of DMFT, see Ref. [24]. For a recent review of the application of DMFT to the electronic structure of the pnictides, see Ref. [4].
[24] A. Georges, G. Kotliar, W. Krauth, and M. J. Rozenberg, Dynamical mean-field theory of strongly correlated fermion systems and the limit of infinite dimensions, Rev. Mod. Phys. **68**, 13 (1996).
[25] S. Biermann, L. de' Medici, and A. Georges, Non-Fermi-Liquid Behavior and Double-Exchange Physics in Orbital-Selective Mott Systems, Phys. Rev. Lett. **95**, 206401 (2005).
[26] H. Ishida and A. Liebsch, Fermi-liquid, non-Fermi-liquid, and Mott phases in iron pnictides and cuprates, Phys. Rev. B **81**, 054513 (2010).
[27] M. Greger, M. Kollar, and D. Vollhardt, Emergence of a Common Energy Scale Close to the Orbital-Selective Mott Transition, Phys. Rev. Lett. **110**, 046403 (2013).
[28] C.-K. Chan, P. Werner, and A. J. Millis, Magnetism and orbital ordering in an interacting three-band model: A dynamical mean-field study, Phys. Rev. B **80**, 235114 (2009).
[29] H. Park, K. Haule, and G. Kotliar, Cluster Dynamical Mean Field Theory of the Mott Transition, Phys. Rev. Lett. **101**, 186403 (2008).
[30] E. Gull, P. Werner, X. Wang, M. Troyer, and A. J. Millis, Local order and the gapped phase of the Hubbard model: A plaquette dynamical mean-field investigation, Europhys. Lett. **84**, 37009 (2008).
[31] H. Lee, Y.-Z. Zhang, H. O. Jeschke, and R. Valentí, Orbital-selective phase transition induced by different magnetic states: A dynamical cluster approximation study, Phys. Rev. B **84**, 020401(R) (2011).
[32] H. Lee, Y.-Z. Zhang, H. O. Jeschke, R. Valentí, and H. Monien, Dynamical Cluster Approximation Study of the Anisotropic Two-Orbital Hubbard Model, Phys. Rev. Lett. **104**, 026402 (2010).
[33] K. S. D. Beach and F. F. Assaad, Orbital-selective Mott transition and heavy-fermion behavior in a bilayer Hubbard model for ^{3}He, Phys. Rev. B **83**, 045103 (2011).
[34] L. De Leo, M. Civelli, and G. Kotliar, $T = 0$ Heavy-Fermion Quantum Critical Point as an Orbital-Selective Mott Transition, Phys. Rev. Lett. **101**, 256404 (2008).
[35] Y. Nomura, S. Sakai, and R. Arita, Nonlocal correlations induced by Hund's coupling: A cluster DMFT study, Phys. Rev. B **91**, 235107 (2015).
[36] K. Bouadim, G. G. Batriuni, and R. T. Scalettar, Determinant Quantum Monte Carlo Study of the Orbitally Selective Mott Transition, Phys. Rev. Lett. **102**, 226402 (2009).
[37] J. Rincón, A. Moreo, G. Alvarez, and E. Dagotto, Exotic Magnetic Order in the Orbital-Selective Mott Regime of Multiorbital Systems, Phys. Rev. Lett. **112**, 106405 (2014).
[38] J. Rinćon, A. Moreo, G. Alvarez, and E. Dagotto, Quantum phase transition between orbital-selective Mott states in Hund's metals, Phys. Rev. B **90**, 241105(R) (2014).
[39] G. Liu, N. Kaushal, S. Li, C. B. Bishop, Y. Wang, S. Johnston, G. Alvarez, A. Moreo, and E. Dagotto, Study of the orbital-selective Mott phases of a one-dimensional three-orbital Hubbard model using computational techniques, Phys. Rev. E **93**, 063313 (2016).
[40] J. M. Caron, J. R. Neilson, D. C. Miller, A. Llobet, and T. M. McQueen, Iron displacements and magnetoelastic coupling in the antiferromagnetic spin-ladder compound $BaFe_2Se_3$, Phys. Rev. B **84**, 180409(R) (2011).
[41] J. M. Caron, J. R. Neilson, D. C. Miller, K. Arpino, A. Llobet, and T. M. McQueen, Orbital-selective magnetism in the spin-ladder iron selenides $Ba_{1-x}K_xFe_2Se_3$, Phys. Rev. B **85**, 180405(R) (2012).
[42] N. D. Patel, A. Nocera, G. Alvarez, R. Arita, A. Moreo, and E. Dagotto, Magnetic properties and pairing tendencies of the iron-based superconducting ladder $BaFe_2S_3$: Combined *ab initio* and density matrix renormalization group study, Phys. Rev. B **94**, 075119 (2016).
[43] S. Dong, J.-M. Liu, and E. Dagotto, $BaFe_2Se_3$: A High T_c Magnetic Multiferroic with Large Ferrielectric Polarization, Phys. Rev. Lett. **113**, 187204 (2014).
[44] Q. Luo, A. Nicholson, J. Rincón, S. Liang, J. Riera, G. Alvarez, L. Wang, W. Ku, G. D. Samolyuk, A. Moreo, and E. Dagotto, Magnetic states of the two-leg-ladder alkali metal iron selenides AFe_2Se_3, Phys. Rev. B **87**, 024404 (2013).
[45] Q. Luo, K. Foyevtsova, G. D. Samolyuk, F. Reboredo, and E. Dagotto, Magnetic states of the five-orbital Hubbard model for one-dimensional iron-based superconductors, Phys. Rev. B **90**, 035128 (2014).
[46] S. R. White, D. J. Scalapino, R. L. Sugar, E. Y. Loh, J. E. Gubernatis, and R. T. Scalettar, Numerical study of the two-dimensional Hubbard model, Phys. Rev. B **40**, 506 (1989).
[47] C.-C. Chang, S. Gogolenko, J. Perez, Z. Bai, and R. T. Scalettar, Recent advances in determinant quantum Monte Carlo, Philos. Mag. B **95**, 1260 (2013).
[48] L. Rademaker, S. Johnston, J. Zaanen, and J. van den Brink, Determinant quantum Monte Carlo study of exciton condensation in the bilayer Hubbard model, Phys. Rev. B **88**, 235115 (2013).
[49] S. R. White, Density Matrix Formulation for Quantum Renormalization Groups, Phys. Rev. Lett. **69**, 2863 (1992).
[50] S. R. White, Density-matrix algorithms for quantum renormalization groups, Phys. Rev. B **48**, 10345 (1993).
[51] E. Y. Loh, Jr., J. E. Gubernatis, R. T. Scalettar, S. R. White, D. J. Scalapino, and R. L. Sugar, Sign problem in the numerical simulation of many-electron systems, Phys. Rev. B **41**, 9301 (1990).
[52] V. I. Iglovikov, E. Khatami, and R. T. Scalettar, Geometry dependence of the sign problem, Phys. Rev. B **92**, 045110 (2015).
[53] K. Bouadim, G. G. Batrouni, F. Hébert, and R. T. Scalettar, Magnetic and transport properties of a coupled Hubbard bilayer with electron and hole doping, Phys. Rev. B **77**, 144527 (2008).

[54] M. Jarrell and J. E. Gubernatis, Bayesian interference and the analytic continuation of imaginary-time quantum Monte Carlo data, Phys. Rep. **269**, 133 (1996).

[55] S. Fuchs, T. Pruschke, and M. Jarrell, Analytic continuation of quantum Monte Carlo data by stochastic analytical inference, Phys. Rev. E **81**, 056701 (2010).

[56] T. D. Kühner and S. R. White, Dynamical correlation functions using the density matrix renormalization group, Phys. Rev. B **60**, 335 (1999).

[57] A. Nocera and G. Alvarez, Spectral functions with the density matrix renormalization group: Krylov-space approach for correction vectors, Phys. Rev. E **94**, 053308 (2016).

[58] O. Akerlund, P. de Forcrand, A. Georges, and P. Werner, Dynamical mean field approximation applied to quantum field theory, Phys. Rev. D **88**, 125006 (2013).

[59] N. Trivedi and M. Randeria, Deviations from Fermi-liquid Behavior Above T_c in 2D Short Coherence Length Superconductors, Phys. Rev. Lett. **75**, 312 (1995).

[60] S. Chi, S. Johnston, G. Levy, S. Grothe, R. Szedlak, B. Ludbrook, R. Liang, P. Dosanjh, S. A. Burke, A. Damascelli, D. A. Bonn, W. N. Hardy, and Y. Pennec, Sign inversion in the superconducting order parameter of LiFeAs inferred from Bogoliubov quasiparticle interference, Phys. Rev. B **89**, 104522 (2014).

[61] A. Lankau, K. Koepernik, S. Borisenko, V. Zabolotnyy, B. Büchner, J. van den Brink, and H. Eschrig, Absence of surface states for LiFeAs investigated using density functional calculations, Phys. Rev. B **82**, 184518 (2010).

[62] H. Eschrig and K. Koepernik, Tight-binding models for the iron-based superconductors, Phys. Rev. B **80**, 104503 (2009).

[63] H. Sakamoto, T. Momoi, and K. Kubo, Ferromagnetism in the one-dimensional Hubbard model with orbital degeneracy: From low to high electron density, Phys. Rev. B **65**, 224403 (2002).

[64] K. Held and D. Vollhardt, Microscopic conditions favoring itinerant ferromagnetism: Hund's rule coupling and orbital degeneracy, Eur. Phys. J. B **5**, 473 (1998).

[65] M. Yi, D. H. Lu, R. Yu, S. C. Riggs, J. H. Chu, B. Lv, Z. K. Liu, M. Lu, Y. T. Cui, M. Hashimoto, S. K. Mo, Z. Hussain, C. W. Chu, I. R. Fisher, Q. Si, and Z. X. Shen, Observation of Temperature-Induced Crossover to an Orbital-Selective Mott Phase in $A_xFe_{2-y}Se_2$ (A = K, Rb) Superconductors, Phys. Rev. Lett. **110**, 067003 (2013).